LIMNOLOGY and OCEANOGRAPHY

ASLO

Limnol. Oceanogr. 66, 2021, 3055–3069

doi: 10.1002/lno.11858

Oxygen-controlled recirculating seepage meter reveals extent of nitrogen transformation in discharging coastal groundwater at the aquifer–estuary interface

Thomas W. Brooks,[1*] **Kevin D. Kroeger**,[1] **Holly A. Michael**,[2,3] **Joanna K. York**[4]

[1]U.S. Geological Survey, Woods Hole Coastal and Marine Science Center, Woods Hole, Massachusetts
[2]Department of Earth Sciences, University of Delaware, Newark, Delaware
[3]Department of Civil and Environmental Engineering, University of Delaware, Newark, Delaware
[4]School of Marine Science and Policy, University of Delaware, Newark, Delaware

Abstract

Nutrient loads delivered to estuaries via submarine groundwater discharge (SGD) play an important role in the nitrogen (N) budget and eutrophication status. However, accurate and reliable quantification of the chemical flux across the final decimeters and centimeters at the sediment–estuary interface remains a challenge, because there is significant potential for biogeochemical alteration due to contrasting conditions in the coastal aquifer and surface sediment. Here, a novel, oxygen- and light-regulated ultrasonic seepage meter, and a standard seepage meter, were used to measure SGD and calculate N species fluxes across the sediment–estuary interface. Coupling the measurements to an endmember approach based on subsurface N concentrations and an assumption of conservative transport enabled estimation of the extent of transformation occurring in discharging groundwater within the benthic zone. Biogeochemical transformation within reactive estuarine surface sediment was a dominant driver in modifying the N flux carried upward by SGD, and resulted in a similar percentage of N removal (~ 42–52%) as did transformations occurring deeper within the coastal aquifer salinity mixing zone (~ 42–47%). Seasonal shifts in the relative importance of biogeochemical processes including denitrification, nitrification, dissimilatory nitrate reduction, and assimilation altered the composition of the flux to estuarine surface water, which was dominated by ammonium in June and by nitrate in August, despite the endmember-based observation that fixed N in discharging groundwater was strongly dominated by nitrate. This may have important ramifications for the ecology and management of estuaries, since past N loading estimates have generally assumed conservative transport from the nearshore aquifer to estuary.

Eutrophication of coastal waterbodies from terrestrial nitrogen loading is a globally widespread occurrence (Howarth et al. 2000). Anthropogenic nutrients, including nitrogen, are transported to coastal waters via atmospheric deposition, surface water inflow, or submarine groundwater discharge (SGD). Within coastal watersheds and aquifers with permeable sediments and high hydraulic conductivity, SGD can be a substantial, and in some cases, predominant vector for nutrients (e.g., Volk et al. 2006). Such groundwater and its associated solutes discharge into coastal waters subaerially through the seepage face, in the nearshore subtidal zone, or farther offshore (e.g., Bokuniewicz 1992). In addition to land-derived fresh groundwater and associated solutes, recirculated saline and brackish groundwater can be important components of SGD (Li et al. 1999; Michael et al. 2005). Seawater is entrained and mixed with fresh groundwater in coastal sediments through processes such as tidal- and wave-pumping, dispersion, and convection (Robinson et al. 2007; Santos et al. 2012), resulting in a biogeochemically reactive salinity transition zone. Depending on the hydrogeological and biogeochemical setting, and redox conditions, biogeochemical processes and transformations occurring in the freshwater aquifer, across salinity gradients in the coastal aquifer, and in overlying estuarine surface sediments, can significantly alter the composition of groundwater along its flowpath. Thus, estimates of nutrient fluxes to coastal waters based on solute concentrations measured in onshore wells can be incomplete.

*Correspondence: wallybrooks@usgs.gov

Additional Supporting Information may be found in the online version of this article.

One approach to address these uncertainties has been to measure subsurface solute concentrations nearshore to assess the extent of biogeochemical alteration across salinity gradients in high spatial resolution with drive-point sampling devices (e.g., Kroeger and Charette 2008; Gonneea and Charette 2014). Although such sampling is a significant improvement, in many coastal settings it may not fully capture the chemistry of water at the point of discharge, as evidence is increasing that biogeochemical processes occurring in the upper few centimeters of organic-rich, biogeochemically reactive estuarine surface sediments, can further alter the composition of the groundwater prior to discharge (Sawyer et al. 2014; Wong et al. 2020). This can have important ecological ramifications, since phytoplankton (including harmful species) preferentially assimilate specific forms of nitrogen, sometimes regardless of the dominant form present (York et al. 2007). For example, it has been shown that ammonium (NH_4^+) promotes growth of dinoflagellates, while nitrate (NO_3^-) promotes growth of diatoms (Taylor et al. 2006). Important processes that might affect the magnitude and speciation of nitrogen fluxes due to small-scale changes in redox conditions include removal from solution as gaseous N_2O, NO, or N_2 by denitrification or anaerobic ammonium oxidation (anammox), fixation, remineralization of organic nitrogen, dissimilatory nitrate reduction to ammonium (DNRA), nitrification, and assimilation by subsurface or benthic microbes. Hence, for accurate understanding of ecosystem response to nutrient loading, it is critical to accurately quantify solute fluxes by direct measurement at the sediment–water interface.

At present, methods are not available to make accurate, direct measurements of the flux of biogeochemically cycled elements and compounds from sediments with groundwater discharge occurring. Measurement of chemical flux under in situ conditions by eddy covariance (e.g., Berg et al. 2003) is advantageous in being nonintrusive, but requires very high sampling frequency (< 1 s) by sensors, and therefore is limited to measurement of solutes that can be quantified in situ at such frequency. Traditional benthic chambers (e.g., Boynton and Kemp 1985) have been modified such that they provide a closer approximation of in situ conditions with regard to light transmission (Point et al. 2007), or O_2-regulation (Morford et al. 2007). However, benthic chambers do not allow groundwater seepage to occur, nor do they allow measurement of seepage, or chemical fluxes associated with seepage. Additionally, it has been demonstrated that thorough mixing of chamber headspace water without sediment resuspension is critical to prevent potentially significant sampling artifacts (Boynton et al. 2018). Traditional (e.g., Lee 1977) and automated (e.g., Paulsen et al. 2001; Rosenberry and Morin 2004) seepage meters directly quantify groundwater-surface water exchange on timescales ranging from days to seconds, and have undergone numerous design changes, improving the reliability and accuracy of the measurements (Rosenberry et al. 2020). However, they cause artifacts in redox conditions, and thus cannot be used to produce reliable measurements of flux of reactive species (Frape and Patterson 1981; Duque et al. 2020). Allowing transmission of photosynthetically active radiation is important because it maintains natural processes including normal growth and assimilation by the microphytobenthos, and oxygen production through photosynthesis. Krupa et al. (1998) and Menheer (2004) developed and evaluated transparent automated seepage meters to allow light transmission and simultaneous measurements of seepage and dissolved constituents. While previous work has provided useful tools and significant advancements, the present study aims to effectively combine the critical conditions required for accurate, direct measurement of the chemical flux.

In this study, a set of linked approaches was employed to measure change in solute flux during groundwater transit from the coastal aquifer, through the benthic zone, and to estuarine surface water, across a range of representative in situ redox conditions. First, two modified seepage meters were employed to directly measure nutrient and trace element fluxes and groundwater discharge across the sediment/estuary interface. A novel O_2- and light-regulated seepage meter (RSM) was designed to maintain light and redox conditions within the RSM similar to overlying estuarine water, provide thorough mixing of headspace water, and measure SGD and associated solute fluxes simultaneously; which to the authors' knowledge, has not been done previously. Additionally, a high-sensitivity ultrasonic sensor was used to measure changes in bidirectional groundwater flux due to variable conditions, such as waves, at 1 s frequency. A standard Lee-type seepage meter (Lee 1977), was deployed alongside the RSM to provide a reference measurement to enable evaluation of the importance and effectiveness of O_2 and light regulation in the RSM. Second, solute concentrations were measured in groundwater samples collected proximal to the seepage meters, enabling endmember-based estimation of advective nutrient and trace element fluxes from the upper coastal aquifer toward the overlying benthic zone and water column. Finally, combining the data and approaches enabled new observations of fluxes and extent of chemical transformation within the upper coastal aquifer and benthic zone, under a range of redox conditions.

Materials and methods

Site description

Field investigations were carried out on the south shore of Guinea Creek, a microtidal estuarine tributary of Rehoboth Bay, situated on a permeable coastal plain aquifer on the Delmarva Peninsula, DE, USA. Sediments of the upper coastal aquifer are comprised of the Pleistocene Beaverdam formation which consists of interbedded sand, silt, clay and gravel deposits (Andres and Ramsey 1996), and are overlain by estuarine silt deposits. Groundwater inputs account for 43–75% of the total N load to Rehoboth Bay, which has been impacted by eutrophication from excess nutrient loading from agricultural and suburban land uses (Volk et al. 2006). The primary focus of the study was on

geochemical conditions and processes occurring in two hydraulically connected but biogeochemically different zones in the nearshore, subtidal SGD zone (Fig. 1). The upper coastal aquifer salinity mixing zone, consisting of the permeable sediments of the Beaverdam formation, hereafter referred to as the "subbenthic zone," was defined as the range of depths from which groundwater was sampled and characterized for the present study (12–45 cm below sediment surface). This zone is characterized by high NO_3^- (~ 250–400 μM), low NH_4^+ (~ 0–10 μM), and relatively high dissolved oxygen (DO, ~ 35–60% saturation) at low salinity (0–3 PSU); with increasing NH_4^+, and decreasing NO_3^- and DO with increasing salinity (Brooks et al. 2021). Reliable groundwater samples could not be obtained shallower than 12 cm below the sediment surface, with the techniques employed in this study. Therefore, we asses geochemical conditions and processes occurring in the top 12 cm, including estuarine sediment with relatively high organic matter content and associated microphytobenthos and microbial biofilms, hereafter "benthic zone," by coupling the water and solute fluxes measured with the seepage meters with an endmember approach based on solute concentrations measured in groundwater at depths of 12–45 cm in the sub-benthic zone. Field measurements, including fluid and solute fluxes measured with seepage meters, groundwater geochemistry, and near-bottom estuarine water quality parameters, were made in June, August, and October of 2015. For the present study, we report results from June and August, the full dataset is available in Brooks et al. (2021). Additional site details are available in Torre et al. (2019), an investigation of phytoplankton community structure responses carried out concurrent to our investigation.

Seepage meters

Two specialized seepage meters were employed in this study to measure SGD and associated solute fluxes under contrasting biogeochemical conditions. The regulated seepage meter (RSM, Fig. 1a) is constructed from a nonreactive stainless steel base and detachable, transparent polycarbonate lid, and occupies a surface area of 0.46 m^2 when deployed into the sediment. The lid allows for transmission of photosynthetically active radiation (> 400 nm); however, certain wavelengths outside of the photosynthetically active spectrum (e.g., ultraviolet) may not be transmitted through the material. The RSM covers a surface area of 0.46 m^2 when deployed into the sediment. Water is continuously recirculated through the seepage meter headspace and the attached sampling loop (total combined volume = 78 L) with a 10 L min^{-1} capacity diaphragm pump—sufficient to provide thorough mixing, but not resuspend or disturb the sediment. Results of a tracer injection test on mix time, described in Supplemental Information Appendix S1, indicated the water contained in the seepage meter headspace and circulation system is 95% mixed within 1.3 min of injection of the tracer (Fig. S1). The circulation system on the RSM includes a syringe port for collection of discrete water samples, an inline YSI 600XLM multiparameter sonde for measurement of salinity, dissolved oxygen (DO), temperature, pH, and oxidation reduction potential (ORP) at 1 min frequency. The flow system includes a 91 m length of gas permeable silicone tubing (9.5 mm inner diameter, 1.6 mm wall thickness) which was kept submerged below the water's surface during field deployment. This length of tubing allows dissolved gas concentrations within the seepage meter, including O_2, to achieve equilibrium with the surrounding water body. These features enable the close approximation of in situ estuarine conditions, and the measurement of representative benthic chemical fluxes.

An ultrasonic flow sensor (FLEXIM F7407; FLEXIM Corp., Edgewood, NY, USA) was deployed in the RSM to capture high temporal resolution (1 s) flow data during the deployments. The ultrasonic transducers were externally mounted onto a manufacturer-recommended 3.5 mm wall thickness, 9.5 mm inner diameter titanium pipe (Fig. 1) for optimal precision in flow measurements. During field deployment, the transducer/pipe assembly was encased in a water-tight rigid plastic polyvinylchloride enclosure and weighted with lead dive weights to achieve a stable and level position when attached to the seepage meter. The sensor was deployed at a depth of up to 1.4 m for a total duration of ~ 24 h, though greater depths and longer duration are achievable. Laboratory and field measurements of instrument performance, including evaluation under low and zero flow conditions, are described in the supplemental information (Figs. S2, S3). Results indicated both excellent precision ($\sigma = 0.07$ cm d^{-1}, $n = 1200$), and excellent agreement to manually measured flows ($r^2 = 1.00$, $p < 0.001$, df = 19), across a range of − 55 to + 75 cm d^{-1}. The minimum flow velocity reported by the manufacturer for the sensor is 1 cm s^{-1}, or the equivalent of 13.3 cm d^{-1} seepage, given the RSM cylinder and flow tube geometry; however, our lab results indicated both excellent precision and accuracy at seepage rates as low as 1.7′ and 0 cm d^{-1}.

The recirculating standard seepage meter (SSM) was constructed to test the hypothesis that isolating the enclosed water column from oxygen renewal and photosynthetically active radiation would result in artifacts in redox conditions and chemical flux. The SSM, modified from Lee (1977) is constructed from the top portion of a 208 L steel drum, and employs a recirculating flow system, discrete sampling port, and inline YSI 600XLM sonde as described above for the RSM (Fig. 1). However, unlike the RSM, the design does not include gas-permeable tubing for oxygen regulation or a transparent lid for transmission of photosynthetically active radiation. The SSM covers a surface area of 0.26 m^2, has a combined headspace + circulation system volume of 21 L, and was operated with a 4 L min^{-1} capacity diaphragm pump. A mixing test of the SSM (Supplemental Information) yielded inconclusive results, however, the theoretical turnover time of water within the SSM and circulation loop based on volume and circulation rate is 21 L/4 L $min^{-1} \approx 5.3$ min, less than that of the RSM

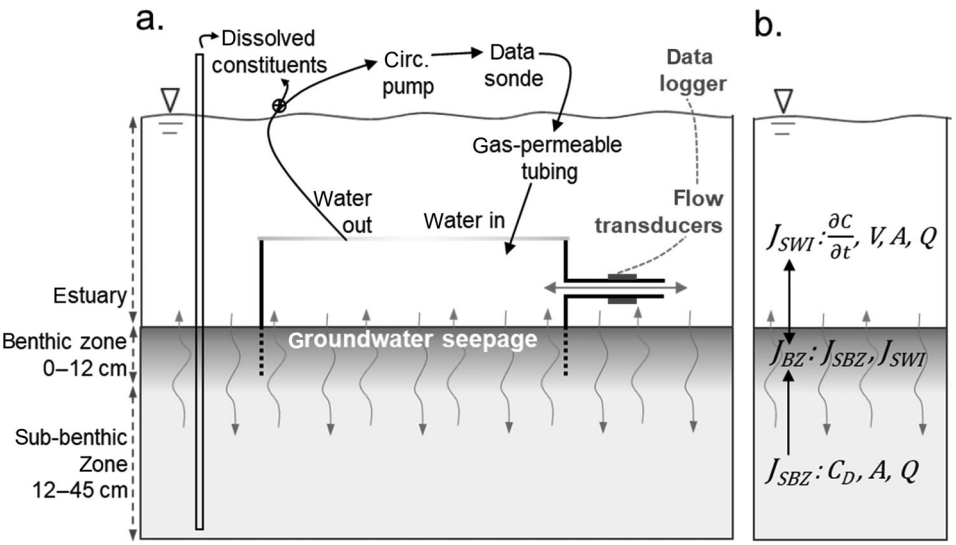

Fig. 1. (**a**) Diagram of the oxygen-regulated ultrasonic seepage meter (RSM) and sampling scheme. Groundwater seepage rate is measured at 1 s frequency with an ultrasonic sensor, or manually within an attached collection bag (not shown). A recirculating flow system mixes headspace water and transports flow to a nearby sampling platform where water quality parameters are measured with an inline multiparameter sonde, and water samples are collected from a syringe port for geochemical analysis. Transmission of photosynthetically active radiation, and regulation of dissolved gases, including O_2, are achieved with a transparent lid and an inline section of gas-permeable tubing. Groundwater samples are collected in the sub-benthic zone with push-point samplers for geochemical analysis, and near-bottom surface water quality parameters and water depth are measured by a multiparameter sonde proximal to the seepage meter (not shown). (**b**) Diagram showing time-averaged chemical fluxes from the sub-benthic zone carried by SGD ($\bar{J}_{SBZ}$, Eq. 3), to or from the benthic zone ($\bar{J}_{BZ}$, Eq. 7), and to or from estuarine surface water ($\bar{J}_{SWI}$, Eq. 6). Necessary parameters include: ∂C, the change in solute concentration within the seepage meter; ∂t, the change in time; Q, the volumetric groundwater seepage rate; C_D, the theoretical solute concentration at a given salinity of discharge; V, the volume of the seepage meter headspace and circulation system; and A, the area of bayfloor occupied by the seepage cylinder. For complete descriptions, *see* Eqs. 3, 6, and 7.

(≈ 7.8 min). Therefore, we anticipate the actual mix time of the SSM to be comparable, or perhaps slightly faster than the RSM.

Sampling methods

The seepage meters were deployed as an adjacent pair (< 1 m separation) in a shoreline-parallel orientation in the nearshore subtidal SGD zone in Guinea Creek, In June, August, and October of 2015 to measure fluid and solute fluxes across the majority or entirety of a single tidal cycle. Deployment location, which was the same for the two deployments reported in the present study, was recorded with a handheld GPS to an accuracy of 2 m or less. Depth of insertion was 15 cm for the RSM and 10.5 cm for the SSM, respectively. Following installation, ample time for hydraulic equilibration (> 45 min) was allowed—it has been shown that for permeable sediments, most of the recovery from disturbed to steady state occurs within 10–30 min following a seepage meter installation (Rosenberry and Morin 2004). During the hydraulic equilibration period, continuous flushing of the seepage meters and flow systems with baywater in an open loop configuration ensured in situ estuarine chemical conditions, including salinity, DO, and other parameters were maintained prior to beginning experimentation. In the case of the RSM, the lid was left detached during this period, while the SSM relied on continuous flushing with the circulation pump. At the end of the equilibration period, the return tube was attached to the intake on the lid of each seepage meter, forming a closed loop. Equivalent in situ starting conditions for the RSM and SSM were confirmed by the close agreement of seepage meter salinity and DO readings to nearby estuarine bottom-water readings.

Discrete water samples were collected from the seepage meters through a syringe port located on the recirculating flow system (Fig. 1a) once the seepage meters were in closed loop mode ($t = 0$), and at regular intervals (30–60 min) during the time series events. Samples were collected into acid-cleaned, sample-rinsed, all-HDPE syringes and subsampled in the field into individual vials for analysis of a suite of dissolved constituents, including: NO_3^-, NH_4^+, dissolved organic carbon (DOC), and trace elements manganese (Mn), and iron (Fe). Trace elements were only collected on a subset of sample points. The total volume of water removed for each set of syringe samples, including that used for rinsing, was recorded and was always 220 mL or less. Immediately upon collection, samples were filtered through sample-rinsed 0.45 μm polyethersulfone disc filters into pre-combusted borosilicate glass vials with teflon-lined septa caps (for DOC) or acid-cleaned HDPE scintillation vials (for remainder of analytes). DOC and trace elements samples were preserved with hydrochloric or

trace metal grade Optima nitric acid, respectively, to pH < 2 and refrigerated until analysis. Samples for nitrate and ammonium were frozen until analysis. Intensive sampling of the RSM and SSM were done concurrently during daytime for a total duration of 9.3 h (June), and 12.3 h (August), the results of which are the primary focus of the present study. Additionally, in June, the RSM was operated overnight past the end of the daytime sampling period to measure in situ nighttime fluxes of the above-listed analytes.

SGD was measured from the seepage meters either ultrasonically (June and October RSM deployments) or manually (all other deployments) through an attached flow tube (Fig. 1a). The inner diameter of flow tubing utilized on both seepage meters is 9.5 mm throughout, regardless of the flow measurement approach used, as resistance to flow is minimal with this design (Koopmans and Berg 2011). The ultrasonic approach most closely followed that of Paulsen et al. (2001); while the manual approach most closely followed Russoniello et al. (2013). For manual measurements, thin-walled plastic collection bags (40 L capacity) were prefilled with ~ 2 L of bay water, to allow measurement of both groundwater discharge and recharge, and to overcome bag resistance to flow (Rosenberry et al. 2008). The prefilled bags were weighed to the nearest 0.05 kg with a digital scale before and after attachment to the seepage meter to quantify the average rate of groundwater flow during each sampling interval, which ranged from 30 to 60 min. Initial and final mass measurements were converted to volumes based on calculated density (Fofonoff and Millard 1983) given additional measured values of temperature and salinity. Measurement of seepage rate via the manual approach did not overlap with time series sampling of water chemistry in the seepage meters. Groundwater flows are reported in units of either volumetric discharge (Q, L h^{-1}), for calculation of absolute fluxes of solutes, or as specific discharge (q, cm d^{-1}) by dividing Q by the area of bay floor covered by the seepage meter ($q = Q/A$), enabling direct comparison of groundwater seepage rates measured in this study, and to other studies.

During the experiments, calibrated YSI 600XLM sondes in flow-through cells recorded salinity, temperature, pH, DO, and ORP in the seepage meters at 1 min frequency. A third YSI 600XLM-V2 sonde, equipped with an optical DO sensor, was deployed ~ 10 cm above the bay floor to measure the near-bottom estuarine parameters listed above, and tidal elevation, at 2 min frequency. Tidal elevation was corrected for elevation of the deployed sensor above the bay floor, and therefore is relative to the bay floor elevation adjacent to the seepage meters. The sondes were calibrated 1 d prior to deployment following manufacturer protocols and cross-checked in the field before and after deployment by simultaneously measuring in a bucket of circulating bay water. We suspect compromised performance of the ORP sensor deployed in the near-bottom water of Guinea Creek in June and August, potentially due to interference from prolonged exposure to reduced material; therefore, estuarine ORP data are not reported. However, despite uncertainty in the accuracy of the absolute readings, ORP data recorded in the seepage meter flow through systems and in groundwater (discussed below), were deemed sufficient for qualitative comparison of the treatments and as a general indicator of redox conditions. ORP values were converted to values of Eh in mV by adding 200 to the values (YSI, Yellow Springs, OH).

Groundwater samples were collected from the sub-benthic zone 12–45 cm below the sediment surface in June ($n = 11$) and August ($n = 13$) to characterize the composition of contributing groundwater in close proximity to the point to discharge, and to estimate advective solute fluxes toward the overlying benthic zone and water column. Samples were collected at multiple depths in vertical profiles, or as individual sample points adjacent to the seepage meter deployments or at locations shoreward within the nearshore, shallow (30–150 cm water depth) subtidal SGD zone. Groundwater was collected with 6 mm outer diameter, 4 cm screened interval, stainless steel push-point samplers (M.H.E. Products, Michigan, USA) and transported with a peristaltic pump to a YSI Pro-Plus multiparameter sonde in a flow-through cell for field measurement of salinity, DO, pH, and ORP. Water was subsampled immediately into individual vials for analysis of NO_3^-, NH_4^+, DOC, and trace elements as described above; however, trace elements and DOC were only collected on a subset of sample points. Interestingly, the distribution of salinity and other solutes did not follow a predictable pattern with respect to depth, potentially due to anisotropic conditions in subsurface sediments, or due to temporal/spatial variation in extent of mixing due to drivers such as tidal or wave pumping, or convection (e.g., Santos et al. 2012). The June and August nitrogen species data were therefore plotted against salinity (range 0–20 PSU during June, and 3–27 PSU during August) and fitted with linear or exponential models to characterize the mixing behavior, and to establish an average endmember concentration in discharging groundwater as later defined in Eq. 3. The predominant mixing behavior (conservative or nonconservative) was designated based on the model of best fit, as determined by the highest coefficient of determination (r^2).

Analytical procedures

Dissolved constituents were analyzed at the University of Delaware in Lewes, DE, USA; and at the US Geological Survey and Woods Hole Oceanographic Institution in Woods Hole, MA, USA. Nitrate and ammonium were analyzed on a Seal AA3 autoanalyzer by the cadmium reduction method, and the phenol hypochlorite method. Nitrate and nitrite were not quantified separately, and their sum is referred to as "NO_3^-" in this manuscript. Dissolved organic carbon was analyzed on an O.I. Analytical Aurora 1030C autoanalyzer by high temperature catalytic oxidation/nondispersive infrared detection (HTCO-NDIR). Trace elements samples were diluted 20-fold

with 5% Optima nitric acid and analyzed on a Thermo Fisher iCAP Qc for total dissolved Mn and Fe. Count rates were normalized to an internal indium (In) standard to account for drift and matrix interference of the solution. Dissolved Fe data from the SSM is not reported due to risk of potential contamination from the seepage meter. Precision of the above-listed analytes, reported as standard error of the mean (SEM), was determined by replicate analysis ($n > 10$) of intermediate concentration calibration standards or natural reference materials. Error terms for benthic and groundwater-derived solute fluxes (described below) were determined by standard error-propagation techniques (Meyer 1975).

Salinity of SGD

The salinity of SGD to the water column can be derived from salinity measurements within the seepage meters by a mass balance approach, considering salt fluxes in and out of the seepage meter, for each time interval i ($S_D[i]$, Eq. 1), or as a time-weighted mean during the measuring period ($\bar{S_D}$, Eq. 2) using the following relationships:

$$S_D(i) = \frac{\frac{\partial S_i}{\partial t_i} V + S_i Q_i}{Q_i} \quad (1)$$

$$\bar{S_D} = \frac{\sum_{i=1}^{n} w_i' \left(\frac{\partial S}{\partial t} V + S_i Q_i\right)}{\sum_{i=1}^{n} w_i' Q_i} \quad (2)$$

where for each sampling interval i, ∂S is the change in salinity within the seepage meter, ∂t is the change in time, S is the average salinity in the seepage meter, Q is the volumetric discharge or recharge rate, V is the volume of the seepage meter headspace and circulation system, and w' is the proportion of sampling interval duration to total deployment duration.

Solute fluxes from the sub-benthic zone

To estimate the fluxes of nutrients and trace elements from sandy sediments of the sub-benthic zone toward the overlying benthic zone and water column carried by SGD, a modified endmember-based approach was applied. This approach relies on the theoretical concentration of a solute, C_D, at a given salinity of discharge, which is defined graphically as the concentration at which the conservative or nonconservative mixing line intersects the calculated $\bar{S_D}$ as obtained from Eq. 2. The resulting time-averaged flux ($\bar{J_{SBZ}}$, Eq. 3), based on measured groundwater advection and either conservative or nonconservative mixing, is defined as:

$$\overline{J_{SBZ}} = \frac{C_D \bar{Q}}{A} \quad (3)$$

where $\bar{Q}$ is the average volumetric groundwater discharge rate, A is the surface area of bayfloor covered by the seepage cylinder, and C_D is the concentration of a given solute at a given salinity of discharge. The standard error for $\bar{J_{SBZ}}$ for NO_3^- and NH_4^+ was calculated based on the root-mean-square error (RMSE) of the predicted value of C_D from the regression.

Groundwater residence time in the benthic zone

The residence time of groundwater in surface sediment within SGD zones is dependent on the rate of SGD, and often exhibits substantial spatial and/or temporal variation (e.g., Sawyer et al. 2014; Russoniello et al. 2018). Residence time controls the contact time of groundwater with sediment particles and associated microbes and may ultimately influence the extent of chemical transformation (e.g., Seitzinger et al. 2006; Wong et al. 2020). We calculated an average residence time for the topmost 12 cm of reactive surface sediment comprising the benthic zone for each deployment of the RSM and SSM based on the estimated volume of the interstitial fluid within the benthic zone sediments and the volumetric groundwater discharge rate, as:

$$\tau = \frac{Az\eta}{\bar{Q}} \quad (4)$$

where z is the thickness of the benthic zone or the vertical distance between the topmost groundwater sample and the bayfloor (= 12 cm, Fig. 1), η is the porosity, and τ is the average residence time in the benthic zone. A typical value for medium sand of $\eta = 0.375$ (Das 2019) was applied, based on sediment present at the study site in the depth range of interest.

Solute fluxes across the sediment–water interface

Fluxes of nutrients and trace elements were measured directly within the RSM and SSM based on a mass balance approach. Given the field setting, the flux represents the net mass flux of the solute due to several potential physical and biogeochemical drivers. This includes advective transport due to upward groundwater advection driven by the hydraulic gradient, surface water/groundwater exchange due to tidal- and wave-pumping (Santos et al. 2012), all of which are captured in seepage meter measurement of fluid flux. Current-bedform interactions (e.g., Huettel et al. 1998) may influence the transport and distribution of solutes and redox conditions within surface sediment, however we suggest this process is negligible in Guinea Creek given continuous upward groundwater seepage, and relatively slow ambient tidal current velocities. The net flux also quantifies biogeochemical drivers influencing production and consumption of the solutes across the sediment–water interface, including the water column contained in seepage cylinder. We suggest that water column transformations likely constitute a relatively small proportion of the total net flux, relative to the low-DO, organic-rich, biogeochemically reactive surface sediment. The flux is expressed per unit area of bayfloor as either an instantaneous flux at each time interval i (Eq. 5), or as a time-averaged flux for the entire deployment (Eq. 6):

$$J_{SWI}(i) = \frac{\frac{\partial C_i}{\partial t_i} V + C_i Q_i}{A} \quad (5)$$

$$\overline{J_{SWI}} = \frac{\sum_{i=1}^{n} w_i' \left(\frac{\partial C}{\partial t} V + C_i Q_i\right)}{A} \quad (6)$$

where for a given sampling interval i, ∂C is the change in concentration of the solute within the seepage meter, ∂t is the change in time, C is the concentration of the solute in the seepage meter, w' is the proportion of the sampling interval duration to total experiment duration, and J_{SWI} is the net flux of the solute across the sediment–water interface. A positive or negative J_{SWI} represents either a net flux from the sediments to the water column, or a net flux from the water column into the sediments, respectively.

Solute fluxes to or from the benthic zone

The time-averaged solute flux representing the net mass change due to advective transport and chemical transformation through the benthic zone ($\bar{J}_{BZ}$, Eq. 7), was calculated as the difference in the endmember-based flux from the subbenthic zone carried by SGD ($\bar{J}_{SBZ}$, Eq. 3) and the net flux across the aquifer–estuary interface ($\bar{J}_{SWI}$, Eq. 6) as measured in the seepage meters, as:

$$\overline{J_{BZ}} = \overline{J_{SBZ}} - \overline{J_{SWI}} \quad (7)$$

Negative and ~ 0 values of $\bar{J}_{BZ}$ indicate net consumption and near-balanced production/consumption across the benthic zone, respectively; and a positive value indicates a net source from the benthic zone.

Specific flux

Since during both June and August in the RSM and SSM, mean q differed, but measured $\bar{S}_D$ (Eq. 2) was approximately equivalent, time-averaged solute fluxes per unit area (Eqs. 3, 6, and 7) were normalized by time-averaged $\bar{q}$ to enable direct comparison of the results of the RSM and SSM. The "specific flux" ($\bar{J}^*$, Eq. 8) is expressed in units of grams or moles of solute per cm of groundwater seepage (e.g., μmol NO_3^- cm^{-1}) using the following relationship:

$$\bar{J}^* = \frac{\bar{J} A}{\bar{q}} \quad (8)$$

where $\bar{J}$ is the average flux per unit area, $\bar{q}$ is average specific discharge rate, and $\bar{J}^*$ is the specific flux of the solute.

Results and discussion

Biogeochemical conditions

In the RSM, DO, temperature, and pH closely approximated near-bottom estuarine conditions both during the daytime experiments (Fig. 2) and under more hypoxic conditions observed at night, indicating that the device can accurately represent a large range of ambient conditions. In June, the RSM experiment ran continuously for ~ 24 h, and average DO concentration was 146% saturation during the daytime, which was within ~ 2% saturation of that measured in nearby estuarine water during the same time period. During nighttime, a lower minimum DO concentration was observed in estuarine water (14%) than in the RSM (46%) indicating that the gas-permeable tubing may have over-oxygenated the water in the RSM. Stratification of DO and other parameters in the water column under calm nighttime conditions could have led to this difference and highlights the need for positioning of the permeable loop closer to the bay floor under conditions when stratification is anticipated. Regardless of this discrepancy, DO concentrations measured in the RSM at night were within the range of nighttime DO concentrations measured in estuarine water, which ranged from 14% to 70% saturation. Therefore, the nighttime RSM observations represent a typical nighttime scenario for Guinea Creek. A similar level of agreement with estuarine water measurements was observed in the August RSM during daytime for DO (within 7% saturation), temperature (within 0.3°C), and pH (within 0.1).

Contrary to patterns observed in the RSM, daytime chemical conditions within the SSM differed significantly from nearby estuarine water composition (Fig. 2), due to the isolation of the water within the seepage meter and sediments beneath it from supply of oxygen and photosynthetically active radiation. Dissolved oxygen decreased in the SSM in both experiments, with a more rapid decrease in August, resulting in a lower minimum concentration in August (1%) vs. June (49%). The pH was also lower on average within the SSM than in estuarine water in June and August (Fig. 2), and decreased gradually over the first few hours of the deployments before stabilizing, pointing to a shift in the balance of production and respiration in the dark, with increases in CO_2 due to respiration driving shifts in pH. Oxidation reduction potential (Eh) also decreased steadily in the SSM, and on average, was ~ 60 and ~ 80 mV for June and August, substantially less than averages of ~ 450 and ~ 390 mV in the RSM. Temperature within the SSM was very similar to both the nearby RSM and estuarine water (within 0.3 °C), limiting any concern that differences in chemical parameters among regulated and standard treatments were due to differences in temperature. Although the redox and light conditions measured within the SSM during the daytime experiments differed from estuarine water, the conditions were similar to the hypoxic nighttime summer conditions measured in nearby estuarine surface water, and to the commonly hypoxic nighttime conditions found during the summer within the Delaware Inland Bays (Tyler et al. 2009). We therefore examined the SSM results as an approximation of nighttime conditions, processes, and fluxes, and contrasted them with light-regulated, oxic conditions observed within the RSM during the daytime. As we will show, spatial and temporal variations in redox conditions within estuarine bottom water can be expected to

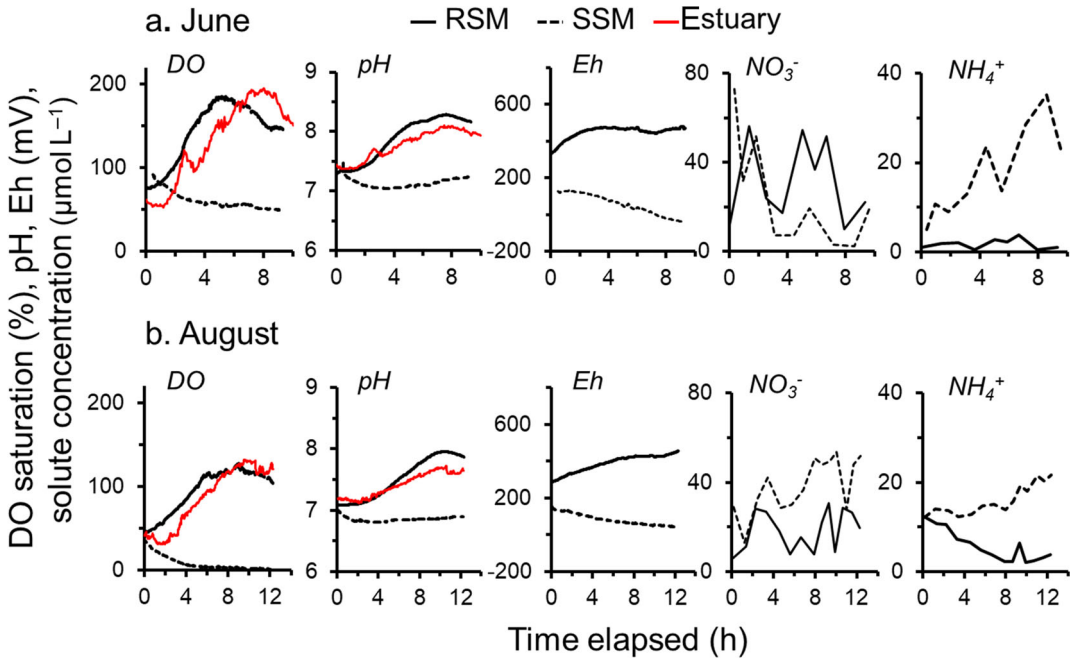

Fig. 2. Dissolved oxygen (DO), pH, Eh, NO_3^-, and NH_4^+ in the regulated seepage meter (RSM, solid black line), standard seepage meter (SSM, dashed black line), and in nearby estuarine bottom water (solid red line) during June (top), and August (bottom) daytime paired deployments. Elapsed time is shown on the *x*-axes. Start times ($t = 0$) were 09:44 h and 08:37 h local time for June and August, respectively. Note that these analytes exhibit significantly different temporal trends depending on the type of seepage meter used.

dramatically alter the magnitude and composition of chemical fluxes carried by SGD.

Submarine groundwater discharge

Net groundwater flow measured manually, and ultrasonically in high resolution revealed patterns occurring across different temporal scales (Fig. 3). Overall, SGD was inversely correlated with tidal elevation, consistent with previous observations from coastal unconfined aquifers (e.g., Lee 1977; Michael et al. 2003), and with expected tidally-driven oscillations in the hydraulic gradient. Ultrasonically measured flows at times indicated large variability in q occurring at shorter timescales (spikes in discharge as high as 25 cm d^{-1} and recharge as high as 4 cm d^{-1}, Fig. 3a). These short periods of enhanced flow predominated during lower tidal stage, and are likely wave-driven benthic exchange (e.g., Russoniello and Michael 2015; Russoniello et al. 2018) resulting from boat wakes observed during field sampling. Less variability is present during calmer conditions, when amplitude of surface water waves and resulting effects on q are expected to be less, such as during the overnight high tide ($t \approx 13$ h, Fig. 3a). Results of an analysis of slope-adjusted ultrasonic q measured during this period (Supplemental Information Appendix S1) show that in situ variability substantially exceeds inherent instrument variability (σ = 0.40 and 0.07 cm d^{-1}, respectively, n = 1200). The variations observed are therefore largely due to changes in the velocity of discharge, possibly due to pressure variations driven by low amplitude, high frequency waves (e.g., Russoniello et al. 2018).

In addition to different scales of temporal variability in SGD observed in groundwater flows, meter-scale differences in the magnitude of SGD, and therefore porewater residence time, were also observed (Fig. 3). Average $\bar{q}$ measured among adjacent deployments of the RSM and SSM were 6.7 and 3.4 cm d^{-1}, respectively, during June, and 4.4 and 9.1 cm d^{-1}, respectively, during August, which correspond to approximate porewater residence times (Eq. 3) of: 0.7, 1.3, 1.0, and 0.5 d, respectively. These differences reflect natural spatial heterogeneity widely observed in natural systems (e.g., Shaw and Prepas 1990; Russoniello et al. 2013), and are not attributable to differences in seepage meter geometry or method of flow measurement approach. Differences in hydraulic conductivity in coastal sediments of the Delaware Inland Bays impact measured seepage rates, and therefore residence times, across a range of spatial scales (Russoniello et al. 2013; Duque et al. 2019), and likely account for the variability observed in Guinea Creek.

Despite the observed spatial variation in the magnitude of $\bar{q}$, average salinity of discharge ($\bar{S_D}$, Eq. 2) did not vary significantly among paired deployments of the RSM and SSM, as indicated by values of 5.5 ± 0.7 and 5.7 ± 0.2 ppt during June; and 10.6 ± 0.9 and 10.5 ± 1.2 ppt during August, respectively.

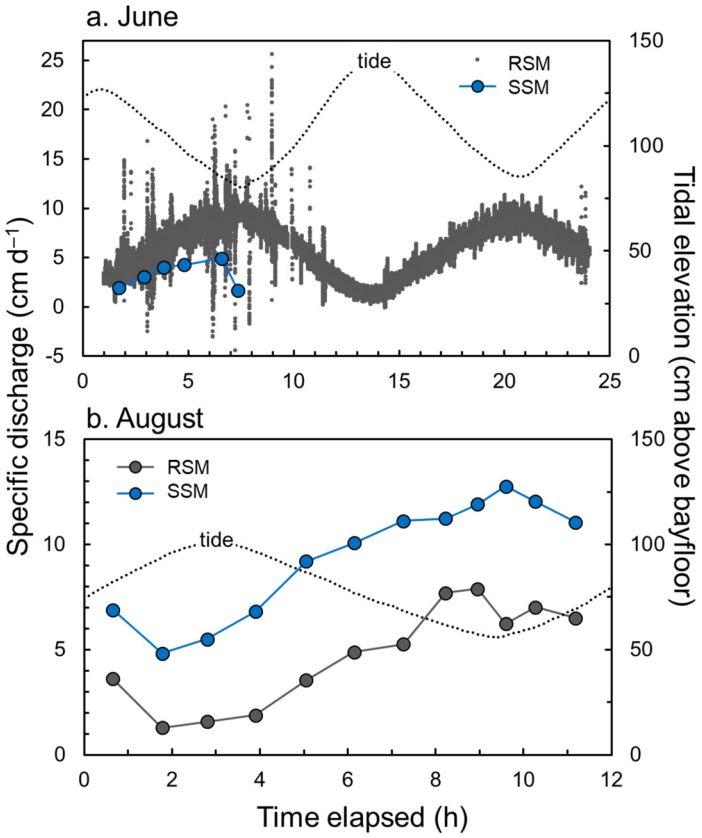

Fig. 3. Time-series of specific discharge (q) measured in the regulated and standard seepage meters (RSM and SSM), and tidal elevation in Guinea Creek in (**a**) June, and (**b**) August of 2015. Ultrasonic q measured in the RSM at 1 s frequency in June is shown in (a) as the dark gray dots. For the other deployments, measurements of q were made manually within an attached collection bag (30–60 min intervals). Elapsed time is shown on the x-axes. Start times ($t = 0$) were 09:44 h and 08:37 h local time for June and August, respectively. Note that scales on axes differ in the two panels.

Differences in discharge salinity from June to August were consistent with salinity differences in contributing groundwater in the sub-benthic zone, which averaged 5.3 ppt in June and 13.0 ppt in August across a similar range of sample depths. The range of salinity among those samples was also lower in June (0–20 ppt) than in August (3–27 ppt), with less midrange salinity. The observed seasonal differences may be explained by a lower water table in August relative to June, which was apparent in a nearby observation well (well I.D. Qi31-03, Delaware Geological Survey online database). This would result in a decrease in the terrestrial hydraulic gradient, a landward shift in the freshwater/saltwater interface, and displacement of fresh groundwater by saline water. Additionally, shorter timescale variations in benthic exchange rate, driven by changes in tidal or wave amplitude (e.g., Russoniello et al. 2018) may partly explain the observed differences in groundwater salinity distributions, and therefore discharge salinity.

Solute trends and fluxes across the sediment–water interface

The NO_3^- and NH_4^+ concentrations measured in the RSM and SSM, regardless of conditions or month sampled, often varied across short timescales, suggesting rapid biogeochemical cycling in the benthic zone and water column (Fig. 2). Despite this variation, NH_4^+ concentrations tended to increase with decreasing DO and Eh in the SSM, resulting in substantially larger fluxes to the overlying water column than observed in the nearby oxic RSM (Table 1). Redox-cycled trace elements Mn and Fe decreased with increasing DO and Eh in the RSM throughout the deployment (Figs. 2, S4), resulting in negative specific fluxes (Table 1) indicating net losses through the benthic zone and water column. In the SSM, Mn increased substantially with decreasing DO and Eh, resulting in large positive fluxes from the benthic zone to overlying water column as expected, due to high solubility under reducing conditions. For comparison, in June, minimum DO saturation measured in the RSM during a nighttime time series (Brooks et al. 2021) was ~ 50%, equivalent to the minimum DO saturation measured in the SSM during daytime (Fig. 2). Time-averaged specific fluxes of Mn, Fe, and NH_4^+ measured during nighttime were approximately 31 μmol cm^{-1}, 46 μmol cm^{-1}, and 286 nmol cm^{-1}—of comparable magnitude with fluxes measured during daytime in the SSM as summarized in Table 1. The conservative constituent salinity decreased steadily through time in both treatments due to upward seepage of fresher groundwater. Salt fluxes measured from the RSM and the SSM, derived from YSI salinity measurements, were in agreement for both June and August (48 ± 1 vs. 40 ± 26, and 105 ± 12 vs. 105 ± 9 g cm^{-1}, Table 1). This is expected due to the conservative nature of chloride, and is an important observation which supports the validity of the measurement approach.

Nitrogen cycling during June

In the sub-benthic zone 12–45 cm below the sediment–water interface, NH_4^+ concentrations, although variable, were low, averaging 4 μM, and were conservative with respect to salinity across a range of 0–20 ppt, Fig. 4. Oxygen saturation was ~ 35–60% in fresh or near-fresh groundwater and reached minima of ~ 3–9% at highest salinity. The low concentrations of NH_4^+ at low-salinity could therefore be explained by a slow rate of microbial mineralization, or removal by nitrification given availability of DO; whereas the higher NH_4^+ concentrations at high-salinity and low-DO may indicate enhanced production via microbial remineralization coupled with decreased consumption via nitrification. The flux of NH_4^+ to the overlying benthic zone as predicted by the endmember approach was ~ 42 μmol cm^{-1}. NO_3^- concentration was relatively high in the fresh and near-fresh groundwater and decreased during mixing with low-NO_3^-, low-DO saline groundwater, resulting in an initial loss of ~ −1021 μmol cm^{-1}, or ~ 48%, across the sub-benthic zone (Figs. 4, 5). The NO_3^- loss mechanisms may

Table 1. Time-averaged specific fluxes (Eq. 8) of biogeochemically reactive (NO_3^-, NH_4^+, and DOC), redox-cycled (Mn and Fe), and conservative (salt) analytes across the sediment–water interface measured during the daytime paired deployments with the light-controlled, oxic regulated seepage meter (RSM), and the suboxic standard seepage meter (SSM). Errors reported are ± 1 SEM. Solute fluxes per unit area can be obtained using the relationship in Eq. 8, and values of A and $\bar{q}$ as stated in the Methods and the Results.

Analyte	Units	Month sampled	RSM-measured specific flux	SSM-measured specific flux
NO_3^-	μmol	Jun	1082 ± 133	−2075 ± 119
	cm^{-1}	Aug	1869 ± 245	792 ± 61
NH_4^+	μmol	Jun	20 ± 219	2049 ± 194
	cm^{-1}	Aug	−718 ± 406	328 ± 98
Mn	μmol	Jun	−37 ± 1	211 ± 3
	cm^{-1}	Aug	−59 ± 3	–
Fe	μmol	Jun	−7 ± 62	–
	cm^{-1}	Aug	−40 ± 150	–
Salt	g cm^{-1}	Jun	48 ± 1	40 ± 26
		Aug	105 ± 12	105 ± 9
DOC	mmol	Jun	10.8 ± 0.4	29.7 ± 0.6
	cm^{-1}	Aug	1.8 ± 0.8	12.1 ± 0.3

include removal via denitrification (e.g., Kroeger and Charette 2008; Colman et al. 2018) or anammox, possibly within reducing microsites (e.g., Sawyer 2015) or assimilation into microbial biomass (e.g., Marchant et al. 2014). Denitrification could have been enabled by available electron donor DOC (e.g., Szymczycha et al. 2017), which was ~ 35–85 μM at lowest salinity and increased to ~ 310–390 μM at high salinity; or by dissolved Fe (Böhlke and Denver 1995), or dissolved Mn (Labbé et al. 2003), both of which followed a similar trend as DOC with respect to salinity (Brooks et al. 2021). Previous

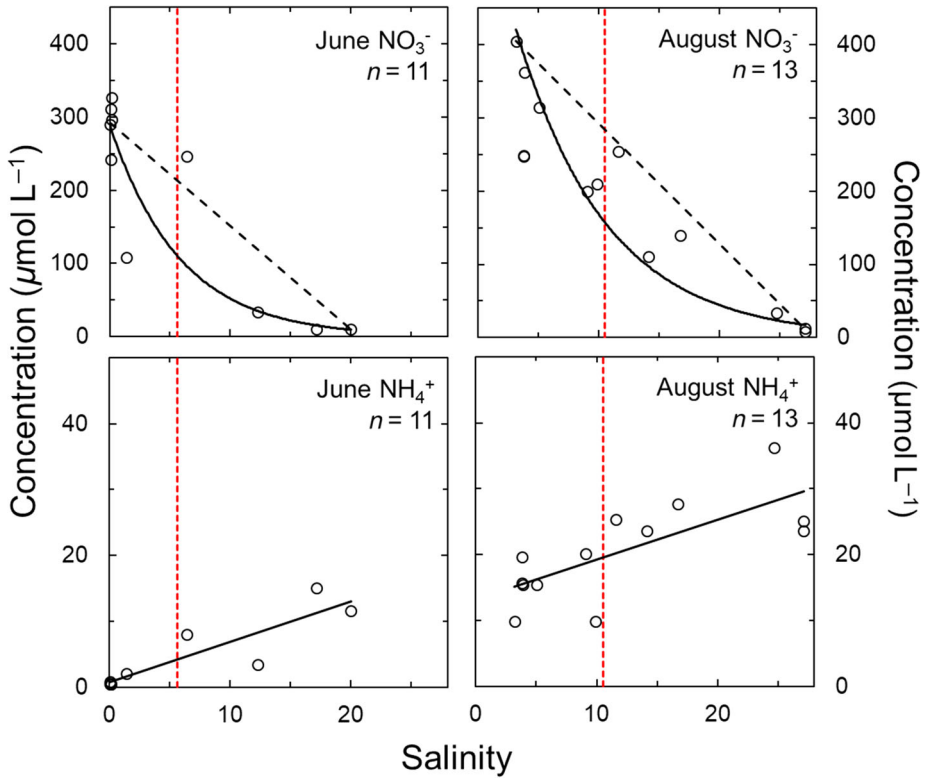

Fig. 4. Groundwater mixing curves for NO_3^- and NH_4^+ in June (left) and August (right) measured in the sub-benthic zone 12–45 cm below the sediment surface. The intersection of the average salinity of discharge ($\bar{S}_D$, Eq. 2, red dashed line) with the mixing curve (solid black line) represents the theoretical concentration of NO_3^- or NH_4^+ in waters discharging to overlying estuarine sediments (C_D).

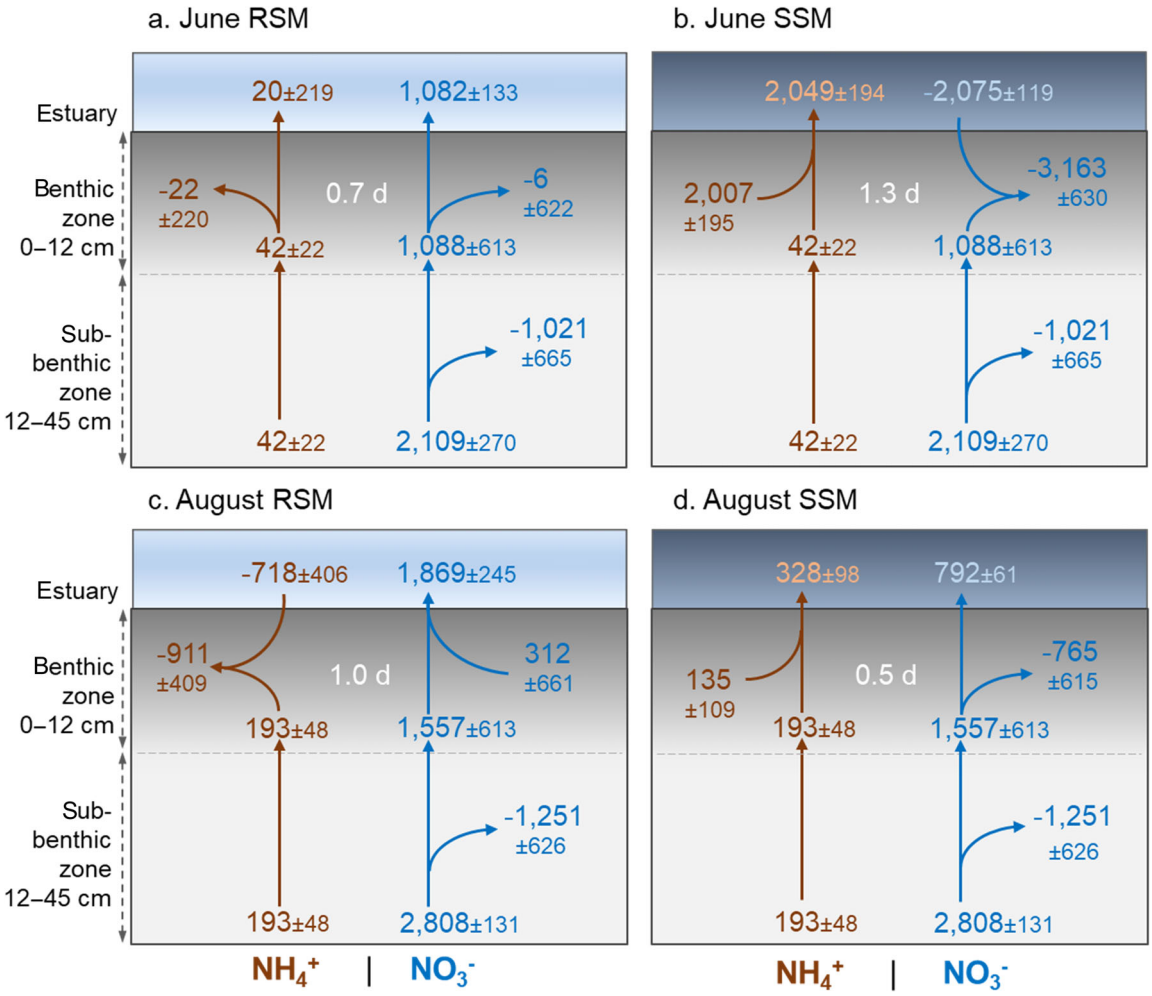

Fig. 5. Schematic diagrams showing specific fluxes (Eq. 8) of NH_4^+ (brown arrows) and NO_3^- (blue arrows) from the sub-benthic zone, to or from the benthic zone, and across the sediment–water interface, under the contrasting redox conditions of the light-controlled, oxic regulated seepage meter (RSM) and suboxic standard seepage meter (SSM) in June (top) and August (bottom). Fluxes are reported in units of μmol solute cm^{-1} groundwater seepage to enable direct comparison of the approaches. Errors reported are ±1SEM. Estimated porewater residence times in the benthic zone (Eq. 4) are also shown in white text.

studies have shown that within coastal sediments, anammox is generally more important where the ratio of NO_3^-: DOC is large (Babbin and Ward 2013), and can remain active even when NH_4^+ concentrations are low, as was the case in the fresh or near-fresh groundwater, but generally decreases in proportion to denitrification in the presence of labile forms of DOC (Smith et al. 2015). The resulting flux of NO_3^- toward the overlying benthic zone accounting for removal via the above-listed pathways was 1088 μmol cm^{-1}.

Under oxic conditions in the RSM (Fig. 5a), the benthic flux of NO_3^- to the water column (Eq. 6, ~ 1082 μmol cm^{-1}) was similar to the endmember-based flux from the sub-benthic zone (Eq. 3, ~ 1088 μmol cm^{-1}), indicating that gains and losses were nearly balanced across the final ~ 12 cm of flow path. Interestingly, the temporally variant NO_3^- concentrations measured in the RSM (Fig. 2) did not correlate to q (not significant, df = 7), indicating that biogeochemical processing was a dominant driver in modifying the efflux. For NH_4^+, the endmember-based flux from the sub-benthic zone (~ 42 μmol cm^{-1}) exceeded the flux to the water column (~ 20 μmol cm^{-1}), indicating a ~ 52% estimated loss in the benthic zone, with no correlation of RSM-measured concentrations to q (not significant, df = 7). Several processes may be active under the conditions present. High oxygen saturation in nearby estuarine surface water (~ 150–200% saturation, Fig. 2a), suggests a high rate of primary productivity and would support assimilation of NH_4^+ and potentially NO_3^- by the microphytobenthos, and promote enhanced nitrification in surface sediments. Additionally, more reducing conditions deeper in the benthic zone could have enabled denitrification or annamox to occur.

Within the hypoxic SSM, NO_3^- and NH_4^+ were inversely correlated during the deployment (Fig. 2, r^2 = 0.79,

$p < 0.0001$, df = 8), and time-averaged fluxes across the sediment–water interface were −2075 and 2049 μmol cm^{-1}, for NO_3^- and NH_4^+ respectively (Fig. 5b). Given fluxes from the sub-benthic zone carried by SGD, this corresponds to a substantial net NO_3^- loss of ~ −3163 μmol cm^{-1}, and a net NH_4^+ addition of ~ 2007 μmol cm^{-1} from the benthic zone. Estuarine surface sediments simultaneously acting as a sink of NO_3^- and a source of NH_4^+ has been observed during sediment core incubations (e.g., York et al. 2010), and may point to several important processes. Removal of NO_3^- and production of NH_4^+ may be explained by DNRA. In contrast, our observations may indicate NO_3^- loss due to denitrification, and NH_4^+ production via remineralization, without coupling to nitrification. All of these processes could be enhanced under highly reducing and O_2-depleted conditions present in the benthic zone, as indicated by low Eh and DO measured in the seepage meter headspace (Fig. 2). Additionally, a slow rate of upward groundwater seepage (3.4 cm d^{-1}) resulted in a residence time of 1.3 d, longer than observed during the other deployments (Fig. 5). A long residence time would increase available time for reaction, and therefore may ultimately increase the extent of transformation in the benthic zone. A large flux of DOC from the benthic zone to the water column (~ 29.7 mmol cm^{-1}, Table 1) relative to a minimal flux from the sub-benthic zone (~ 0.27 mmol cm^{-1}) points to a high concentration of DOC in surface sediment. This condition could enhance DNRA, as past studies have shown that DNRA can increase in relative importance to denitrification when the ratio of available carbon as an electron donor to NO_3^- increases (Marchant et al. 2014). However, we would need to track these changes more directly in future studies to determine which processes were dominant.

Nitrogen cycling during August

As in June, NO_3^- behaved nonconservatively in the sub-benthic zone in August across a salinity range of 3–27 ppt (Fig. 4). Along with higher average salinity in groundwater samples in August (12 ppt) than in June (4 ppt), average DO and average Eh were both lower (24% and −72 mV) than in June (42% and −27 mV). Despite these differences, the mixing behavior of NO_3^- in August was similar to June, with a similar percentage loss (~ 45%) observed. However, the resulting estimated flux of NO_3^- to the overlying benthic zone was larger in August (~ 1557 μmol cm^{-1}) than during June (~ 1088 μmol cm^{-1}), owing to the slightly higher theoretical concentration at discharge (C_D, Fig. 4). NH_4^+, although more variable, behaved conservatively (Fig. 4), and concentrations were, on average, higher in August (~ 21 μmol L^{-1}) than during June (~ 4 μmol L^{-1}). The higher NH_4^+ concentrations in August were likely the result of a higher rate of production via remineralization, while nitrification may have been inhibited by lower DO concentrations than measured earlier in the season. The resulting estimated flux of NH_4^+ from the sub-benthic zone to the overlying estuarine sediments in August was substantially larger than during June at ~ 193 μmol cm^{-1}.

Under oxic conditions in August (Fig. 5c), the benthic zone was a larger sink for NH_4^+ from both the sub-benthic zone (~ −193 μmol cm^{-1}) and water column (~ −718 μmol cm^{-1}) than under similar conditions in June, resulting in a net flux to the benthic zone (~ −911 μmol cm^{-1}) that was greater than that observed in June by a factor of ~ 40. Concurrently, the flux of NO_3^- to the water column (~ 1869 μmol cm^{-1}) exceeded the flux from the sub-benthic zone (~ 1557 μmol cm^{-1}), indicating a shift from near balanced losses and gains in June, to a net addition (~ 312 μmol NO_3^- cm^{-1}) from the benthic zone to the water column in August. Despite this observation, NO_3^- concentrations measured in the RSM during the deployment, like during the June RSM and SSM deployments, were erratic and not correlated to q (not significant, df = 10), indicating that biogeochemical processing in the benthic zone was a dominant driver in modifying the efflux. Changes in the relative availability of NH_4^+ and NO_3^- could have resulted in a shift in the preferential form of N assimilated by primary producers. In the water column, Dugdale et al. (2012) found that NH_4^+ must be 4 μM or less for phytoplankton to take up NO_3^-. A shift from NO_3^- and NH_4^+ assimilation in June to strictly NH_4^+ assimilation in August, as was observed, seems possible given that average NH_4^+ concentration in groundwater discharging to the benthic zone (C_D, Fig. 4), and in surface water (Fig. 2) was at or below that threshold in June, but above it in August. Additionally, the shifts could also partly be the result of an enhanced rate of nitrification, given higher concentrations of NH_4^+ in the water column and in contributing groundwater in August, or due to the potential for increased biogeochemical processing resulting from the longer residence time in August (1 d) relative to June (0.7 d).

As observed in June, the benthic zone was a sink for NO_3^- and a source of NH_4^+ under hypoxic conditions in the SSM in August (Fig. 5d). However, the magnitudes of these fluxes were smaller than in June, indicating a decreased rate of NO_3^- loss and decreased rate of NH_4^+ production in the benthic zone prior to discharge. For example, ~ 100% of the NO_3^- flux from the sub-benthic zone was transformed in the benthic zone in June, relative to ~ 50% in August. In June, NH_4^+ production in the benthic zone was the dominant source to the total efflux to the water column (approaching ~ 100%), whereas in August, the contribution from the benthic zone constituted ~ 40% of the total efflux (Fig. 5). A decreased rate of DNRA in the benthic zone relative to denitrification could account for much of the observed seasonal shift, since, contrary to June, coupled NO_3^- loss/NH_4^+ production was not apparent in headspace concentration trends through time (not significant, df = 13, Fig. 2). These observations may also be explained by the higher $\bar{q}$ during August (9.1 cm d^{-1}), which resulted in a shorter residence time of SGD in the benthic zone in August SSM (0.5 d) relative to the June SSM (1.3 d). This would reduce the available time for transformation and therefore may be expected to limit the extent of transformations affecting NO_3^- and NH_4^+, including

denitrification, DNRA, remineralization, and assimilation. Consistent with our observations in situ, in flow-through reactor experiments, Wong et al. (2020) observed that both high flow rates (short residence time), and high initial concentrations correlated with a lower fraction of NO_3^- consumed through coastal sediments.

Implications for diurnal and seasonal variation

Since geochemical conditions measured in the light-controlled, oxic RSM and the suboxic SSM (Fig. 2) approximated conditions in nearby estuarine water conditions during daytime, and nighttime, respectively, a chemical flux integrated across the contrasting redox conditions of the RSM and the SSM may approximate a typical diurnal redox cycle, and therefore approximates the "true flux" to Guinea Creek, or similarly impacted estuaries. In comparing the integrated true flux across sampling month, we estimate that transformations of NO_3^- in the subbenthic zone (including removal via denitrification and anammox) reduces the total dissolved inorganic N ($NO_3^- + NH_4^+$) flux to the overlying benthic zone by ~ 47% in June and ~ 42% in August. This loss estimate is consistent with numerous past observations of removal via denitrification in subsurface salinity mixing zones (e.g., Kroeger and Charette 2008; Colman et al. 2018; Wong et al. 2020). Furthermore, transformations occurring in the benthic zone and enclosed water column (potentially including denitrification, nitrification, DNRA, remineralization, and assimilation) further reduce the dissolved inorganic N flux to the estuary by ~ 52% in June and ~ 42% in August. This results in total estimated dissolved inorganic N reductions of ~ 75% and ~ 62%, respectively. However, these losses understate the extreme impact of the methodological differences in our estimates. For example, while the endmember approach estimates the composition of the flux to be dominated by NO_3^- regardless of season (~ 96% and ~ 89% for June and August, respectively), the true flux in June was entirely dominated by NH_4^+, with a net influx of NO_3^- from the water column into sediment. This may be attributed to greater extent of NO_3^- consumption (denitrification and DNRA) and NH_4^+ production (remineralization and DNRA) in the benthic zone. Opposite to June, In August, the true flux was entirely NO_3^-, with a net influx of NH_4^+ from the water column into sediment (Fig. 5). This pattern may be attributed to a greater extent of net NH_4^+ consumption (increased nitrification, increased assimilation, reduced DNRA) and net NO_3^- production (increased nitrification, reduced DNRA). To understand the relative contributions of these processes influencing the extent of production and consumption, we would need track these processes more directly.

Conclusions

These results demonstrate that maintaining in situ biogeochemical conditions is critical to accurately quantify flux of reactive species through estuarine sediment carried by SGD, and that previously and widely applied sampling approaches may miss alterations of the chemical load as it fluxes toward the estuary. Biogeochemical transformation within reactive estuarine surface sediment was a dominant driver in modifying the N flux carried upward by SGD, and resulted in a similar percentage of N removal (~ 42–52%) as did transformations occurring deeper within the sub-benthic zone (~ 42–47%). Past overestimation of the flux of N to estuarine surface water by an endmember approach may indicate that estuaries are more sensitive to N loads than previously indicated, and may have implications for total maximum daily load (TMDL) allocation (Shirmohammadi et al. 2006). The speciation of N in waters discharging through surface sediment to the overlying water column varied with season, dominated by NH_4^+ in June, and NO_3^- in August. This seasonal variation in speciation may have important ecological ramifications, as it may either promote or impede the proliferation of specific phytoplankton, including potentially harmful species. These new types of data indicate that eutrophication status as a driver of benthic redox conditions can be expected to dramatically alter the rate and composition of net nitrogen flux in SGD zones. Clearly, there is a need to better understand the influence of diurnal and seasonal cycles on the extent of chemical transformation, since the true flux that is relevant to the eutrophication status of an estuary will be determined by processes at all time scales.

References

Andres, A. S., and K. W. Ramsey. 1996. Geology of the Seaford area, Delaware. Delaware Geological Survey Report of Investigations No. 53.

Babbin, A. R., and B. B. Ward. 2013. Controls on nitrogen loss processes in Chesapeake Bay sediments. Environ. Sci. Technol. **47**: 4189–4196. doi:10.1021/es304842r

Berg, P., H. Røy, F. Janssen, V. Meyer, B. B. Jørgensen, M. Huettel, and D. De Beer. 2003. Oxygen uptake by aquatic sediments measured with a novel non-invasive eddy-correlation technique. Mar. Ecol.: Prog. Ser. **261**: 75–83. doi:10.3354/meps261075

Böhlke, J. K., and J. M. Denver. 1995. Combined use of groundwater dating, chemical, and isotopic analyses to resolve the history and fate of nitrate contamination in two agricultural watersheds, Atlantic coastal plain, Maryland. Water Resour. Res. **31**: 2319–2339. doi:10.1029/95WR01584

Bokuniewicz, H. J. 1992. Analytical descriptions of subaqueous groundwater seepage. Estuaries **15**: 458–464. doi:10.2307/1352390

Boynton, W. R., and W. M. Kemp. 1985. Nutrient regeneration and oxygen consumption by sediments along an estuarine salinity gradient. Mar. Ecol.: Prog. Ser. **23**: 45–55. doi:10.3354/meps023045

Boynton, W. R., M. A. Ceballos, E. M. Bailey, C. L. Hodgkins, J. L. Humphrey, and J. M. Testa. 2018. Oxygen and nutrient exchanges at the sediment–water interface: A global

synthesis and critique of estuarine and coastal data. Estuaries Coasts **41**: 301–333. doi:10.1007/s12237-017-0275-5

Brooks, T. W., K. D. Kroeger, H. A. Michael, B. Szymczycha, M. J. Eagle, and J. K. York. 2021. Nearshore groundwater seepage and geochemical data measured in 2015 at Guinea Creek, Rehoboth Bay, Delaware. U.S. Geological Survey Data Release. doi:10.5066/P94NBY3Z

Colman, J. A., and others. 2018. Geochemical conditions and nitrogen transport in nearshore groundwater and the subterranean estuary at a Cape Cod embayment, East Falmouth, Massachusetts, 2013–14. US Geological Survey Scientific Investigations Report 2018-5095. 10.3133/sir20185095

Das, B. M. 2019. Advanced soil mechanics. CRC Press.

Dugdale, R., F. Wilkerson, A. E. Parker, A. Marchi, and K. Taberski. 2012. River flow and ammonium discharge determine spring phytoplankton blooms in an urbanized estuary. Estuar. Coast. Shelf Sci. **115**: 187–199. doi:10.1016/j.ecss.2012.08.025

Duque, C., K. Knee, C. J. Russoniello, M. Sherif, O. Aborisha, N. C. Sturchio, and H. A. Michael. 2019. Characterizing small-scale spatial variability of radium isotopes in submarine groundwater discharge. J. Hydrol. **579**: 124192. doi:10.1016/j.jhydrol.2019.124192

Duque, C., C. J. Russoniello, and D. Rosenberry. 2020. History and evolution of seepage meters for quantifying flow between groundwater and surface water: Part 2—marine settings and submarine groundwater discharge. Earth Sci. Rev. **204**: 103168. doi:10.1016/j.earscirev.2020.103168

Fofonoff, N. P., and R. C. Millard Jr. 1983. Algorithms for the computation of fundamental properties of seawater. UNESCO Technical Papers in Marine Sciences 44: 53.

Frape, S. K., and R. J. Patterson. 1981. Chemistry of interstitial water and bottom sediments as indicators of seepage patterns in Perch Lake, Chalk River, Ontario. Limnol. Oceanogr. **26**: 500–517. doi:10.4319/lo.1981.26.3.0500

Gonneea, M. E., and M. A. Charette. 2014. Hydrologic controls on nutrient cycling in an unconfined coastal aquifer. Environ. Sci. Technol. **48**: 14178–14185. doi:10.1021/es503313t

Howarth, R. W., and others. 2000. Nutrient pollution of coastal rivers, bays, and seas. Issues Ecol. **7**: 1–16.

Huettel, M., W. Ziebis, S. Forster, and G. W. Luther III. 1998. Advective transport affecting metal and nutrient distributions and interfacial fluxes in permeable sediments. Geochim. Cosmochim. Acta **62**: 613–631. doi:10.1016/S0016-7037(97)00371-2

Koopmans, D., and P. Berg. 2011. An alternative to traditional seepage meters: Dye displacement. Water Resour. Res. **47**: W01506. doi:10.1029/2010WR009113

Kroeger, K. D., and M. A. Charette. 2008. Nitrogen biogeochemistry of submarine groundwater discharge. Limnol. Oceanogr. **53**: 1025–1039. doi:10.4319/lo.2008.53.3.1025

Krupa, S., T. Belanger, H. Heck, J. Brock, and B. Jones. 1998. Krupaseep—the next generation seepage meter. J. Coastal Res. **26**: 210–213.

Labbé, N., S. Parent, and R. Villemur. 2003. Addition of trace metals increases denitrification rate in closed marine systems. Water Res. **37**: 914–920. doi:10.1016/S0043-1354(02)00383-4

Lee, D. R. 1977. A device for measuring seepage flux in lakes and estuaries 1. Limnol. Oceanogr. **22**: 140–147. doi:10.4319/lo.1977.22.1.0140

Li, L., D. A. Barry, F. Stagnitti, and J. Y. Parlange. 1999. Submarine groundwater discharge and associated chemical input to a coastal sea. Water Resour. Res. **35**: 3253–3259. doi:10.1029/1999WR900189

Marchant, H. K., G. Lavik, M. Holtappels, and M. M. Kuypers. 2014. The fate of nitrate in intertidal permeable sediments. PLoS One **9**: e104517. doi:10.1371/journal.pone.0104517

Menheer, M. A. 2004. Development of a benthic-flux chamber for measurement of ground-water seepage and water sampling for mercury analysis at the sediment–water interface. U.S. Geological Survey Scientific Investigations Report 2004-5298.

Meyer, S. L. 1975. Data analysis for scientists and engineers. Wiley.

Michael, H. A., J. S. Lubetsky, and C. F. Harvey. 2003. Characterizing submarine groundwater discharge: A seepage meter study in Waquoit Bay, Massachusetts. Geophys. Res. Lett. **30**: 1297. doi:10.1029/2002GL016000

Michael, H. A., A. E. Mulligan, and C. F. Harvey. 2005. Seasonal oscillations in water exchange between aquifers and the coastal ocean. Nature **436**: 1145–1148. doi:10.1038/nature03935

Morford, J. L., W. R. Martin, L. H. Kalnejais, R. François, M. Bothner, and I. M. Karle. 2007. Insights on geochemical cycling of U, Re and Mo from seasonal sampling in Boston Harbor, Massachusetts, USA. Geochim. Cosmochim. Acta **71**: 895–917. doi:10.1016/j.gca.2006.10.016

Paulsen, R. J., C. F. Smith, D. O'Rourke, and T. F. Wong. 2001. Development and evaluation of an ultrasonic ground water seepage meter. Groundwater **39**: 904–911. doi:10.1111/j.1745-6584.2001.tb02478.x

Point, D., M. Monperrus, E. Tessier, D. Amouroux, L. Chauvaud, G. Thouzeau, and J. Clavier. 2007. Biological control of trace metal and organometal benthic fluxes in a eutrophic lagoon (Thau Lagoon, Mediterranean Sea, France). Estuar. Coast. Shelf Sci. **72**: 457–471. doi:10.1016/j.ecss.2006.11.013

Robinson, C., L. Li, and D. A. Barry. 2007. Effect of tidal forcing on a subterranean estuary. Adv. Water Resour. **30**: 851–865. doi:10.1016/j.advwatres.2006.07.006

Rosenberry, D. O., and R. H. Morin. 2004. Use of an electromagnetic seepage meter to investigate temporal variability in lake seepage. Groundwater **42**: 68–77. doi:10.1111/j.1745-6584.2004.tb02451.x

Rosenberry, D. O., J. W. LaBaugh, and R. J. Hunt. 2008. Use of monitoring wells, portable piezometers, and seepage meters to quantify flow between surface water and ground water, p. 39, 4–70, D2. *In* D. O. Rosenberry and J. W. LaBaugh [eds.], Field techniques for estimating water fluxes between surface water and ground water. US Geological Survey Techniques and Methods.

Rosenberry, D. O., C. Duque, and D. R. Lee. 2020. History and evolution of seepage meters for quantifying flow between groundwater and surface water: Part 1—freshwater settings. Earth Sci. Rev. **204**: 103167. doi:10.1016/j.earscirev.2020.103167

Russoniello, C. J., and H. A. Michael. 2015. Investigation of seepage meter measurements in steady flow and wave conditions. Groundwater **53**: 959–966. doi:10.1111/gwat.12302

Russoniello, C. J., C. Fernandez, J. F. Bratton, J. F. Banaszak, D. E. Krantz, A. S. Andres, L. F. Konikow, and H. A. Michael. 2013. Geologic effects on groundwater salinity and discharge into an estuary. J. Hydrol. **498**: 1–12. doi:10.1016/j.jhydrol.2013.05.049

Russoniello, C. J., J. W. Heiss, and H. A. Michael. 2018. Variability in benthic exchange rate, depth, and residence time beneath a shallow coastal estuary. J. Geophys. Res.: Oceans **123**: 1860–1876. doi:10.1002/2017JC013568

Santos, I. R., B. D. Eyre, and M. Huettel. 2012. The driving forces of porewater and groundwater flow in permeable coastal sediments: A review. Estuar. Coast. Shelf Sci. **98**: 1–15. doi:10.1016/j.ecss.2011.10.024

Sawyer, A. H. 2015. Enhanced removal of groundwater-borne nitrate in heterogeneous aquatic sediments. Geophys. Res. Lett. **42**: 403–410. doi:10.1002/2014GL062234

Sawyer, A. H., O. Lazareva, K. D. Kroeger, K. Crespo, C. S. Chan, T. Stieglitz, and H. A. Michael. 2014. Stratigraphic controls on fluid and solute fluxes across the sediment–water interface of an estuary. Limnol. Oceanogr. **59**: 997–1010. doi:10.4319/lo.2014.59.3.0997

Seitzinger, S., J. A. Harrison, J. K. Böhlke, A. F. Bouwman, R. Lowrance, B. Peterson, C. Tobias, and G. V. Drecht. 2006. Denitrification across landscapes and waterscapes: A synthesis. Ecol. Appl. **16**: 2064–2090. doi: 10.1890/1051-0761(2006)016[2064:dalawa]2.0.co;2

Shaw, R. D., and E. E. Prepas. 1990. Groundwater-lake interactions: I. Accuracy of seepage meter estimates of lake seepage. J. Hydrol. **119**: 105–120. doi:10.1016/0022-1694(90)90037-X

Shirmohammadi, A., and others. 2006. Uncertainty in TMDL Models. Trans. ASABE **49**: 1033–1049. doi:10.13031/2013.21741

Smith, R. L., J. K. Bohlke, B. Song, and C. R. Tobias. 2015. Role of anaerobic ammonium oxidation (anammox) in nitrogen removal from a freshwater aquifer. Environ. Sci. Technol. **49**: 12169–12177. doi:10.1021/acs.est.5b02488

Szymczycha, B., K. D. Kroeger, J. Crusius, and J. F. Bratton. 2017. Depth of the vadose zone controls aquifer biogeochemical conditions and extent of anthropogenic nitrogen removal. Water Res. **123**: 794–801. doi:10.1016/j.watres.2017.06.048

Taylor, G. T., C. J. Gobler, and S. A. Sañudo-Wilhelmy. 2006. Speciation and concentrations of dissolved nitrogen as determinants of brown tide *Aureococcus anophagefferens* bloom initiation. Mar. Ecol.: Prog. Ser. **312**: 67–83. doi:10.3354/meps312067

Torre, D. M., K. J. Coyne, K. D. Kroeger, and J. K. York. 2019. Phytoplankton community structure response to groundwater-borne nutrients in the Inland Bays, Delaware, USA. Mar. Ecol.: Prog. Ser **624**: 51–63. doi:10.3354/meps13012

Tyler, R. M., D. C. Brady, and T. E. Targett. 2009. Temporal and spatial dynamics of diel-cycling hypoxia in estuarine tributaries. Estuaries Coasts **32**: 123–145. doi:10.1007/s12237-008-9108-x

Volk, J. A., K. B. Savidge, J. R. Scudlark, A. S. Andres, and W. J. Ullman. 2006. Nitrogen loads through baseflow, stormflow, and underflow to Rehoboth Bay, Delaware. J. Environ. Qual. **35**: 1742–1755. doi:10.2134/jeq2005.0373

Wong, W. W., A. Applegate, S. C. Poh, and P. L. Cook. 2020. Biogeochemical attenuation of nitrate in a sandy subterranean estuary: Insights from two stable isotope approaches. Limnol. Oceanogr. **65**: 3098–3113. doi:10.1002/lno.11576

York, J. K., G. Tomasky, I. Valiela, and D. J. Repeta. 2007. Stable isotopic detection of ammonium and nitrate assimilation by phytoplankton in the Waquoit Bay estuarine system. Limnol. Oceanogr. **52**: 144–155. doi:10.4319/lo.2007.52.1.0144

York, J. K., G. Tomasky, I. Valiela, and A. E. Giblin. 2010. Isotopic approach to determining the fate of ammonium regenerated from sediments in a eutrophic sub-estuary of Waquoit Bay, MA. Estuaries Coasts **33**: 1069–1079. doi:10.1007/s12237-010-9278-1

Acknowledgments

We thank Dan Torre, Beata Szymczycha, Stephanie DeVries, and Meagan Eagle for field and/or analytical support. Chris Russoniello and Carlos Duque provided valuable comments on the preparation of this manuscript. We thank Don Rosenberry (USGS) and two anonymous reviewers for their constructive and valuable comments. Any use of trade, firm, or product names is for descriptive purposes only and does not imply endorsement by the U.S. Government. This work was supported by an award from Delaware Sea Grant (award No. NA100AR4170084 to J.K.Y. and K.D.K.), and by the USGS Coastal and Marine Hazards and Resources Program.

Conflict of Interest

None declared.

Submitted 04 November 2020
Revised 05 April 2021
Accepted 11 May 2021

Associate editor: Perran Cook